Precision measurement of the absolute energy of the $2s3s\ ^1S_0$ state in neutral ^{9}Be

K. J. Ahrendsen, T. Karani, and W. D. Williams*
Physics Department, Smith College, Northampton, Massachusetts 01063, USA

(Received 29 July 2024; revised 31 August 2024; accepted 6 September 2024; published 23 September 2024)

We report on the absolute energy of the $2s3s\ ^1S_0$ state in neutral ^{9}Be. In doing so, we measure the transition frequencies of the $2s^2\ ^1S_0 \rightarrow 2s2p\ ^1P_1^\circ$ and $2s2p\ ^1P_1^\circ \rightarrow 2s3s\ ^1S_0$ transitions, also determining the absolute energy of the $2s2p\ ^1P_1^\circ$ state. The results are obtained from a home-built hollow cathode discharge lamp using saturated absorption spectroscopy with laser frequencies referenced to a frequency comb. The transition frequencies are determined to be 1 276 080 080(50) and 363 105 650(130) MHz for the $2s^2\ ^1S_0 \rightarrow 2s2p\ ^1P_1^\circ$ and $2s2p\ ^1P_1^\circ \rightarrow 2s3s\ ^1S_0$ transitions, respectively. The absolute energies are determined to be 42 565.4498(17) and 54 677.350(5) cm^{-1} for the $2s2p\ ^1P_1^\circ$ and $2s3s\ ^1S_0$ states, respectively. The results confirm recent theoretical calculations that included α^6 (QED) corrections. All experimental results are limited by unresolved hyperfine structure.

DOI: 10.1103/PhysRevA.110.032818

I. INTRODUCTION

Quantum electrodynamics (QED) is currently the best theory describing the interactions between charged particles. While extremely successful, there are a variety of theoretical approaches that are used to model these interactions, each with their own challenges. Broadly, there are two pathways to expand our understanding of QED: We can either perform high-energy experiments, such as the $g-2$ experiment [1] and electron-positron collider experiments [2,3], or conduct high-precision measurements in atoms or molecules [4]. Both types of experiments look for discrepancies between the theory and experimental results.

Over the past few decades, light atoms have served as a testing bed for QED. Initial experimental measurements conducted with the intention to test QED effects focused on few-body systems such as helium [5,6] and highly charged heliumlike ions [7]. For the initial theoretical work on these systems, the Slater- or Hylleras-type basis functions were used, which account for electron correlation effects in the wave function. However, these techniques did not easily translate to atoms with more electrons as integrating these basis functions is computationally expensive and each added electron dramatically increases the number of integrals [8]. The most recent theoretical results including QED effects on four- or more-electron systems have been published using explicitly correlated Gaussian basis sets, or the ECG method [9]. Though these basis sets do not fulfill the cusp condition, they make up the difference in computational simplicity [10]. For a recent overview of theoretical developments for the light atoms, see Refs. [11,12]. In brief, QED corrections to absolute transition frequencies have been included for transitions in up to five-electron systems. Apart from studying QED, spectroscopy on these light elements across their isotope chain involving s orbitals will also play a critical role in the development of microscopic nuclear theory [13–16].

This work measures the absolute energy of the $2s3s\ ^1S_0$ state through measurement of the transition frequencies for the $2s^2\ ^1S_0 \rightarrow 2s2p\ ^1P_1^\circ$ transition and the $2s2p\ ^1P_1^\circ \rightarrow 2s3s\ ^1S_0$ transition in neutral ^{9}Be, a four-electron system. The previous best experimental measurement of the absolute energy of the $2s3s\ ^1S_0$ state, reported by Johansson [17], was 54 677.26(10) cm^{-1}, or an uncertainty of 3 GHz. Since that time, three theoretical results have been published [11,18,19], all consistent with one another and the most precise [11] an order of magnitude more accurate than the experiment at 54 677.35(1) cm^{-1}. The work has been completed by two different research groups who both use the ECG method but differ in how they account for the finite mass of the nucleus, resulting in slightly different results.

In each of the publications, agreement with the experimental result from Johansson was achieved after the inclusion of both α^5 and α^6 QED corrections, which shifted the calculated value by about 0.5 and 0.02 cm^{-1}, respectively. Though the theory agreed with experiment, the uncertainties on the theoretical calculations were up to 10 times more precise, motivating further experimental precision. Only a more precise experimental measurement can confirm or refute whether the α^6 corrections were of an appropriate magnitude.

The states involved in determining the $2s3s\ ^1S_0$ state energy are outlined in the Grotrian diagram shown in Fig. 1. These transitions were all initially measured by Paschen *et al.* [22] and then updated by Johansson [17], who used a hollow cathode discharge. The $2s^2\ ^1S_0 \rightarrow 2s2p\ ^1P_1^\circ$ transition, referred to as the 235-nm transition for the rest of this paper, was recently measured by Cook *et al.* using an atomic beam [23]. The transition frequency, referenced to a calibrated ultralow expansion cavity [24], was determined to be 1 276 080 092(40) MHz. These results, which were limited by unresolved hyperfine structure, are in agreement with the most recent theoretical calculations [25,26]. This paper presents experimental results obtained using a different setup, detailed in Sec. II, with the

*Contact author: wraven@smith.edu

 ©2024 American Physical Society

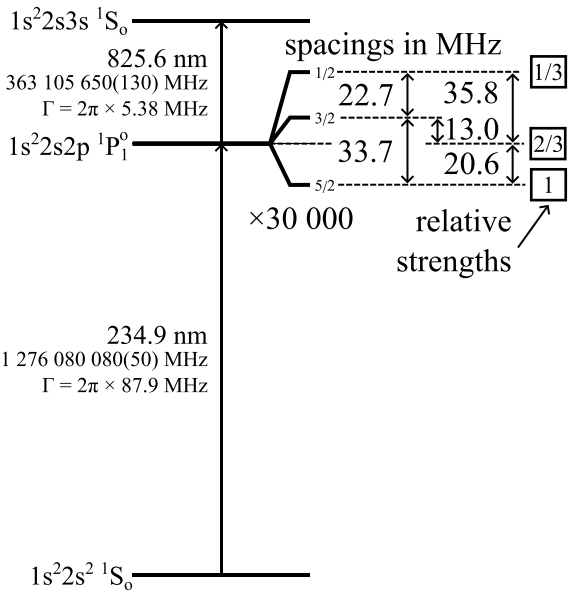

FIG. 1. Grotrian diagram of the relevant transitions and levels involved in the measurements presented in this paper. The frequencies of the transitions are from the results of this paper. The natural linewidths were obtained from the NIST database [20]. Hyperfine spacings are obtained using the A and B constants of Puchalski *et al.* [21]. The relative strengths are normalized to the strongest transition, which is given a value of unity.

laser frequency calibrated by a frequency comb. To confirm the reliability and accuracy of our setup, we first remeasure this transition. The $2s2p\,^1P_1^\circ \rightarrow 2s3s\,^1S_0$ transition, referred to as the 825-nm transition for the rest of this paper, was most recently measured by Johansson to have a frequency of 363 205 400(600) MHz [17,20]. It has also been calculated [26] and the values are consistent.

Be^9 has a nuclear spin quantum number of $I = 3/2$ resulting in hyperfine structure. Both the ground state and the $2s3s\,^1S_0$ state have $J = 0$ indicating a single hyperfine level with designation $F = 3/2$. However, the $2s2p\,^1P_1^\circ$ state has three closely spaced hyperfine levels. The magnetic dipole and electric quadrupole hyperfine constants were recently calculated by Puchalski *et al.* to be $A = -13.8882(7)$ MHz and $B = 0.845\,40(4)$ MHz [21], respectively, resulting in the hyperfine splitting indicated in Fig. 1. Due to the large natural linewidth of the $2s2p\,^1P_1^\circ$ state of $\Gamma = 2\pi \times 87.9$ MHz and the closely spaced hyperfine levels, neither the 235-nm transition nor the 825-nm transition has resolved hyperfine structure.

This paper presents results on the absolute energy of the $2s3s\,^1S_0$ state that improve on the experimental precision by a factor of 20 and are consistent with and a factor of 2 more precise than the most recent theoretical calculations. The paper is organized as follows. Section II gives an overview of the experimental setups for both the 235-nm experiment and the 825-nm experiment. Section III presents the experimental results as well as a discussion of uncertainties and possible future experiments to further improve precision. A brief summary is provided in Sec. IV.

II. EXPERIMENTAL SETUP

Spectroscopic measurements are performed on gaseous beryllium that is produced in an argon gas sustained discharge, produced using a home-built hollow cathode lamp. The lamp, whose dimensions are reported in Ref. [27], is modeled with small modifications from the designs from Refs. [28,29]. The lamp consists of two grounded stainless-steel anodes and a cathode held at a negative voltage. The cathode is composed of a stainless-steel cylinder holding a beryllium cylinder. The discharge is driven by biasing the cathode using a power supply (Kepco BOP 500M) operating in constant current mode. We find pressures above 200 mTorr are required to initiate the discharge and it continues to operate at pressures up to 4000 mTorr.

The laser absorption is monitored with a standard saturated absorption spectroscopy setup, shown in the inset of Fig. 2. The pump beam is amplitude modulated at 314.15 kHz using an acousto-optical modulator (AOM). For the 235-nm experiment, the AOM has a resonant frequency of 80 MHz (Brimrose FQM-150-5-235), while the AOM for the 825-nm experiment (IntraAction Corp. AOM-40) has a resonant frequency of 40 MHz. The positive sideband is used for both experiments, resulting in a frequency-shifted spectrum that is accounted for during analysis. The transmission of the probe beam is monitored using a photodiode (Thorlabs PDA10A for the 235-nm experiment and Thorlabs PDA36A for the 825-nm experiment). The voltage output of the photodiode is demodulated at the pump beam modulation frequency using a lock-in amplifier (Stanford Research Systems SR865A). The resultant Doppler-free spectrum is recorded by LabVIEW software on a computer.

The laser light is provided by a Ti:sapphire laser (MSquared). Light for the 825-nm experiment is used directly from the output of the Ti:Sapphire laser. Light for the 235-nm experiment is produced at 940 nm and sent through a series of two doubling cavities to obtain the 235-nm light. For both experiments, a portion of the infrared light is used for both stabilization and control of the laser frequency. The laser is stabilized to a frequency comb (Toptica DFC CORE +) that is referenced to an atomic clock (SRS FS740) to provide absolute transition frequencies. The stabilization is achieved by using a proportional-integral-derivative controller to maintain the beat frequency f_{beat} between the laser and the nearest comb mode at a level determined by the an electronically adjustable rf bandpass filter. When locked, the uncertainty on the laser frequency is approximately 1 kHz. Due to experimental limitations, the control of the frequency is different for the two experiments.

A. The 235-nm experiment

For the 235-nm experiment, the 940-nm light is stabilized and scanned in the same manner as in Refs. [12,30], diagramed in Fig. 2 as method 1. Method 1 adjusts the laser frequency by scanning the frequency of an AOM. The portion of light used for control is sent to a double-pass AOM with a resonant frequency of 800 MHz (Brimrose GPM-800-200), which shifts the frequency of the light by 1600 ± 300 MHz. Then only the frequency-shifted light is sent to the frequency comb after being amplified (ThorLabs BOA930S).

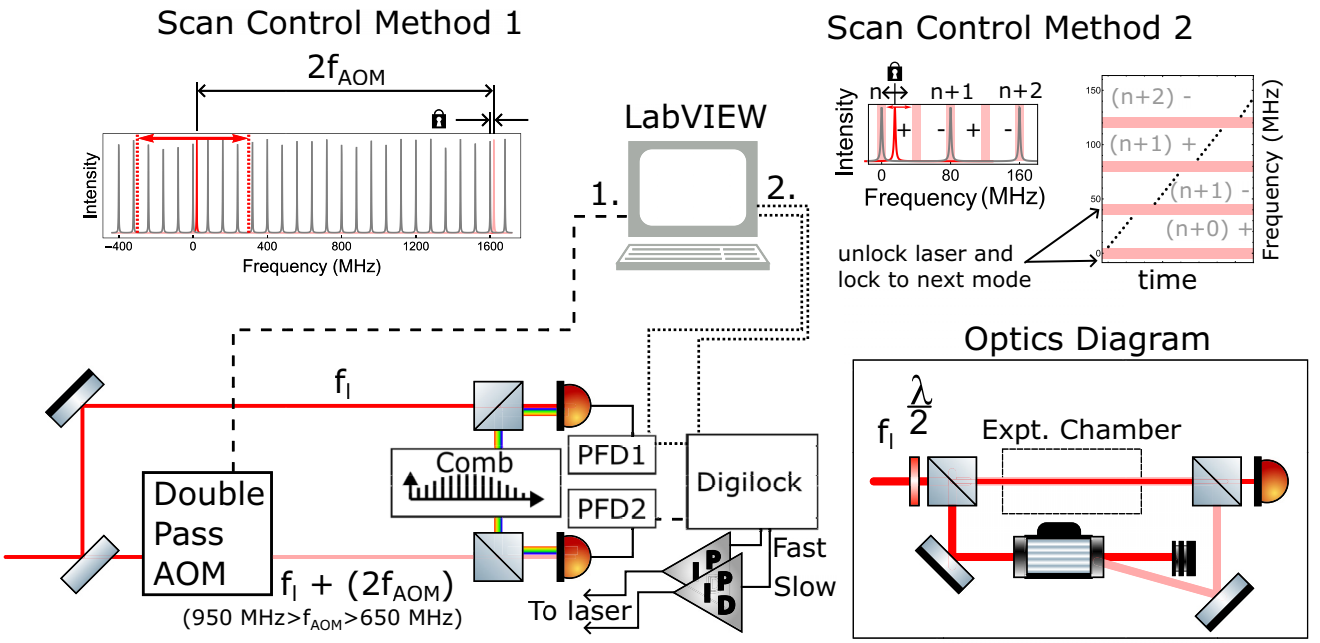

FIG. 2. Laser control and optics setup for the experiment. Scan control method 1 was used for the 235-nm transition, where the double-pass AOM shifted light is locked to a nearby frequency comb mode and the double-pass AOM frequency is adjusted to scan the laser frequency. Scan control method 2 was used for the 825-nm transition, where the laser was scanned by directly adjusting the locking position relative to the comb mode. Here PFD denotes phase and frequency detector.

The relationship between the laser frequency $f_{\mathrm{L},235}$ and the control frequencies is given by

$$f_{\mathrm{L},235}(f_{\mathrm{AOM}}) = 4(nf_{\mathrm{rep}} + 2f_{\mathrm{AOM}} + f_{\mathrm{beat}}), \tag{1}$$

where n is the comb number that was determined using a wavemeter (High-Finesse/Angstrom WS7-30), $f_{\mathrm{rep}} = 80$ MHz is the repetition rate of the comb, $2f_{\mathrm{AOM}}$ is twice the frequency driving the AOM, and $f_{\mathrm{beat}} = 20$ MHz is the beat note between the nearest frequency comb mode and the shifted laser light. The factor of 4 is due to the frequency quadrupling of the laser light for the 235-nm experiment. The frequency of the light probing the beryllium atoms is controlled by changing f_{AOM}. Referring again to Fig. 2, the shifted light, shown in light red, is locked to be f_{beat} from the nearest comb mode, shown in gray. The AOM driving frequency is scanned, and the locking feedback adjusts the frequency of the unshifted light, shown in red, to maintain the validity of Eq. (1). The AOM has a suitable bandwidth to scan the laser frequency over the entire spectrum.

The details of the scan at 235 nm are as follows. The f_{AOM} is adjusted in 1-MHz steps, resulting in a spacing between data points of 8 MHz. At each frequency, the program pauses for 60 ms (the lock-in amplifier time constant is 10 ms) before averaging the output of the lock-in amplifier for 0.2 s and recording this value and the discharge pressure to the data file. The background pressure is 250 mTorr for the measurement.

The discharge power supply operates in constant current mode at -13 mA and approximately -300 V. Larger currents or voltages would result in complete absorption of the probe beam. The probe laser power is 70 μW and the pump laser is approximately 240 μW. The presented data are obtained by averaging data from seven different scans collected under identical experimental conditions.

B. The 825-nm experiment

We could not use the same scanning method to study the 825-nm transition. The damage threshold of the AOM crystal and the efficiency limit of the AOM dictate that the available laser power after the second pass through the AOM is on the order of microwatts, which is too small for use by the frequency comb. The fiber amplifier used for the 235-nm experiment only operates between 900 and 960 nm, so a new scanning method needed to be developed.

For the 825-nm experiment, the laser frequency is adjusted by changing the frequency of the locking point of the laser (f_{beat}) to values between 5 and 35 MHz offset from the comb mode (see method 2 in Fig. 2). At frequencies higher than 35 MHz and lower than 5 MHz the error signal produced by f_{beat} becomes distorted, reducing the accuracy of the lock. This is indicated by the light red regions in the plots. A LabVIEW program automates the process of unlocking the laser and adjusting the frequency to the adjacent stable region. For example, the laser is first locked to the positive side of the frequency comb mode n, indicated by $(n + 0)+$ in Fig. 2, and scanned (f_{beat}) over the stable range. After the stable region is scanned, the laser is relocked to the negative side of the next frequency comb mode, indicated as $(n + 1)-$ in Fig. 2. This process is repeated until the full frequency range of the transition is covered. The equation relating the laser frequency and the control frequencies is then

$$f_{\mathrm{L},825}(n, f_{\mathrm{beat}}) = nf_{\mathrm{rep}} + f_{\mathrm{beat}}. \tag{2}$$

As with the 235-nm experiment, the frequency comb mode number is determined by a wavemeter. Therefore, the frequency of the light probing the beryllium atoms is controlled by changing f_{beat} while recording n.

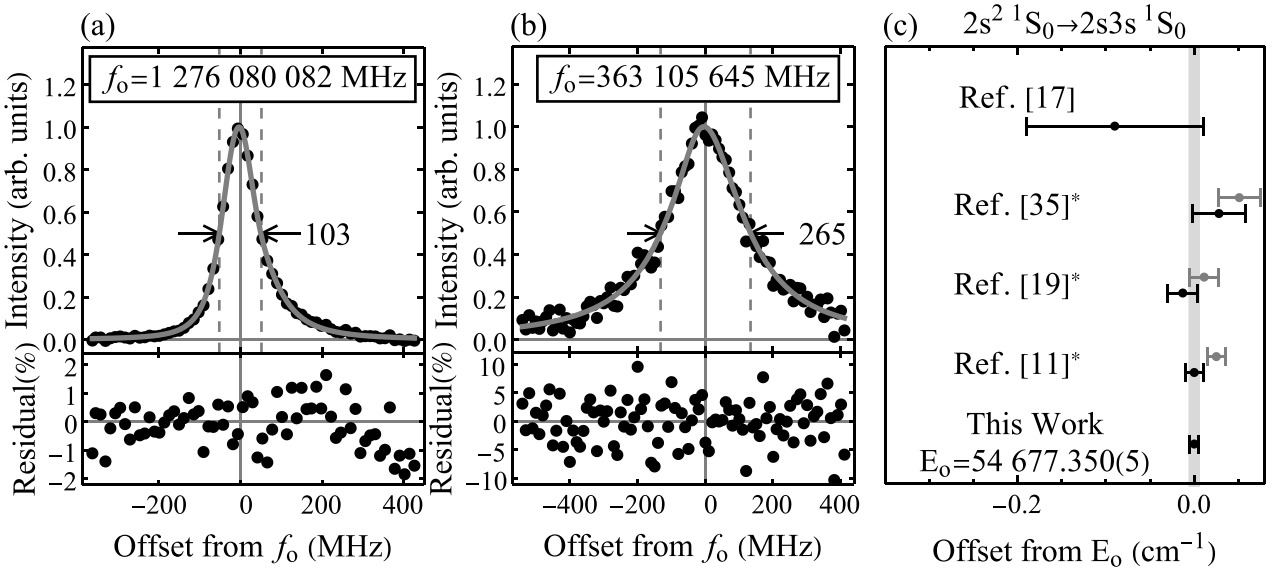

FIG. 3. (a) Example spectrum for $2s^2\ ^1S_0 \rightarrow 2s2p\ ^1P_1^\circ$. (b) Example spectrum for $2s2p\ ^1P_1^\circ \rightarrow 2s3s\ ^1S_0$. (c) Absolute energy of the $2s3s\ ^1S_0$ state. The asterisk indicates calculations, which also display data points in gray indicating the value obtained with only α^5 corrections. The result from Ref. [11] did not include the intermediate error bar for the α^5 correction, so we used the overall uncertainty of the final result, which should be larger than the uncertainty for the α^5 correction.

The atomic signal for the 825-nm experiment is weaker than that for the 235-nm experiment due to several factors. The lower level for the 825-nm transition has a lifetime of 1.8 ns [20], reducing the number of atoms available for spectroscopy. Additionally, the natural linewidth of the 825-nm transition is $2\pi \times 5.38$ MHz, compared to $2\pi \times$ 87.9 MHz for the 235-nm transition. Consequently, several adjustments to the data collection procedure are implemented.

For the 825-nm transition, the measurements are performed as follows. Data are collected in frequency steps of 10 MHz. The program pauses for 300 ms before recording the light intensity to avoid hysteresis effects in the scan (the lock-in amplifier time constant is 30 ms). To observe a suitable signal-to-noise ratio, the output of the lock-in amplifier is averaged for 500 ms. The discharge pressure needs to be larger (roughly 1500 mTorr) and the discharge current is held at the maximum current of −80 mA with a voltage of approximately −340 V. The probe and pump powers are 4 and 19 mW, respectively.

III. RESULTS AND DISCUSSION

Example spectra for the two experiments are shown in Fig. 3. For the 235-nm experiment, there is a total of six spectral features in Fig. 3(a). Three of these features represent real transitions while the other three are from V-style crossovers. For the 825-nm experiment, shown in Fig. 3(b), the lower state has three hyperfine levels with a short lifetime of 1.8 ns. This short lifetime should suppress possible Λ-type crossovers. However, other transitions between two excited states in other elements have been shown to have Λ crossovers despite having a short-lived lower level [31,32]. Therefore, this transition could also have up to six spectral features. The hyperfine constants for the $2s2p\ ^1P_1^\circ$ state, which determine the size of the spacing between these features, were calculated by Pachucki *et al.* [21] and are shown in Fig. 1.

Fitting such complicated spectra poses several challenges. First, there exist quantum interference effects due to closely spaced hyperfine levels [12,33,34]. This complicates fitting by removing possible constraints on the relative strengths and hyperfine splittings for the real transitions. Second, the amplitude of crossover features is difficult to estimate. Finally, the laser's polarization can introduce optical pumping effects, altering the expected amplitudes of the real transitions.

Due to the overlapping spectral features, fitting the spectrum to a sum of six Lorentzian functions without constraints on the amplitudes or widths, but assuming known hyperfine splitting calculated from the hyperfine constants from Pachucki *et al.* [21], leads to unrealistic results for some fit parameters like the amplitudes and widths of the spectral features, correlation matrices with large off-diagonal elements, and uncertainties in the center-of-gravity frequency on the order of 3 MHz. Constraining the model by allowing up to 20% variation in expected relative amplitudes of the real transitions, constraining the amplitudes of the crossover transitions to twice the maximum recorded intensity, and permitting up to 20% variation in the widths of the spectral features produces suitable fits and residuals and more realistic uncertainties on the center-of-gravity frequencies on the order of 15 MHz [see Figs. 3(a) and 3(b) for examples using these fitting conditions]. However, we find that the uncertainty of the extracted center-of-gravity frequency is highly dependent on the initial values of the free parameters and the amount of relaxation of the constraints.

For this reason, we have low confidence in the value and uncertainty obtained through fitting the spectra to a physical model. Still, the close resemblance of even the most rudimentary of our tested models to the experimental data indicates that the center of gravity lies near the peak intensity of the spectrum. We therefore adopt a more conservative determination of the transition frequency, following the

TABLE I. Most recent theoretical and experimental results for the transitions and energy level studied in this paper. The asterisk indicates theoretical results.

Source	Value (cm^{-1})	Value (MHz)
	235 nm	
Ref. [25]*	42 565.441(11)	1 276 079 820(330)
Ref. [23]	42 565.4501(13)	1 276 080 090(40)
Ref. [26]*	42 565.443(9)	1 276 079 880(270)
Present work	42 565.4498(17)	1 276 080 080(50)
	825 nm	
Ref. [17]	12 111.909(30)	363 105 900(900)
Ref. [26]*	12 111.906(5)	363 105 810(120)
Present work	12 111.901(4)	363 105 650(130)
	$2s3s\,^1S_0$ absolute energy	
Ref. [17]	54 677.26(10)	
Ref. [35]*	54 677.378(30)	
Ref. [19]*	54 677.337(17)	
Ref. [11]*	54 677.35(1)	
Present work	54 677.350(5)	

technique outlined in Refs. [12,23]. We use the model with 20% constraints described above to fit the spectrum, but only to determine the peak intensity. Next the frequencies of the two half-maximum values on either side of the maximum are found, effectively finding the full width at half maximum of the spectral feature. The center-of-gravity transition frequency is given as the average of those two frequencies, while the uncertainty is half the difference.

Using the methodology discussed above, we estimate the center-of-gravity frequency for the 235-nm transition to be 1 276 080 080(50) MHz. This result is consistent with the slightly more precise results from our group [23] and the latest theoretical predictions [26], confirming both the previous findings and the viability of the experimental setup. The transition frequency for the 825-nm transition is determined to be 363 105 650(130) MHz, improving on previous experimental results by an order of magnitude. This updated experimental value also agrees with the most recent theoretical results [26].

To confirm that pressure shifts are negligible compared to the above uncertainties, spectra are taken at multiple pressures. For the 235-nm transition, the spectral feature shifts by +20 MHz when the argon pressure is increased from 250 mTorr to 1300 mTorr. For the 825-nm transition, changing the pressure from 930 mTorr to 2300 mTorr shifts the peak of the spectral feature by −20 MHz. Assuming the pressure shifts are linear across the pressure range, these shifts are small enough that when added in quadrature with given uncertainties of the center of gravity they are negligible.

By combining these two measurements we can obtain the absolute energy of the $2s3s\,^1S_0$ state. We find that value to be 54 677.350(5) cm^{-1}, a factor of 20 improvement over previously reported experimental values [17,20]. It also agrees with and is a factor of 2 more precise than the most recent theoretical results [11]. The most recent results are summarized in Fig. 3 and Table I.

Improving the precision of these results will require new experimental setups, given the difficulties in fitting described above. To obtain a more precise value for the transition frequency of the 235-nm transition, a setup must address both crossovers and quantum interference effects. Quantum interference effects can be mitigated by studying beryllium in an atomic beam with the laser propagation direction perpendicular to that of the atomic beam. With this geometry and with the laser polarization oriented at the so-called magic angle, both quantum interference effects and crossovers can be avoided [33,34].

A second approach is to simplify the fitting model by performing crossover-free saturated absorption spectroscopy [36]. This reduces the number of spectral features in the fitting model from 6 to 3 and should aid in obtaining a well-specified fit. However, this method requires two independently tunable 235-nm lasers. Additionally, the hyperfine separation of the excited state will still result in a merged spectrum.

To increase the precision of the absolute energy of the upper state, a two-photon off-resonance transition at 365.8 nm or a Raman transition can be used to excite atoms directly from the ground state. This approach eliminates any broadening from the middle state, producing a spectral feature with a width on the order of the natural linewidth of the excited state, which is 5.38 MHz. However, these transitions require either a high laser intensity or a sufficiently large signal from ground-state gaseous beryllium, which presents its own challenges.

IV. CONCLUSION

In this paper we have described saturated absorption spectroscopy measurements to obtain the absolute energy of the neutral ^{9}Be $2s3s\,^1S_0$ state. This was accomplished through measuring the transitions $2s^2\,^1S_0 \rightarrow 2s2p\,^1P_1^\circ$ and $2s2p\,^1P_1^\circ \rightarrow 2s3s\,^1S_0$. The result for the absolute frequency for the former is consistent with previous results that used atomic beam spectroscopy. The latter measurement improved on the previous experimental uncertainty and agrees with the most recent theoretical results. By combining the results of the two transitions, we calculated the absolute energy of the $2s3s\,^1S_0$ state and found agreement with theoretical predictions while improving on the precision of the previous experimental result by a factor of 20. This measurement confirms that the α^5 and α^6 QED corrections included in the theoretical calculations are accurate. Since the α^6 QED correction produced a shift 25 times smaller than the α^5 QED correction, it is likely that subsequent higher-order QED contributions will surpass the precision of current experimental methods. This underscores the need for both experimentalists and theorists to continue refining their work.

The data supporting this paper are available from the authors upon reasonable request.

ACKNOWLEDGMENTS

This work was supported by the National Science Foundation through Grants No. PHY-1555232 and No. PHY-2110311.

[1] D. P. Aguillard, T. Albahri, D. Allspach, A. Anisenkov, K. Badgley, S. Baeßler, I. Bailey, L. Bailey, V. A. Baranov, E. Barlas-Yucel, T. Barrett, E. Barzi, F. Bedeschi, M. Berz, M. Bhattacharya, H. P. Binney, P. Bloom, J. Bono, E. Bottalico, T. Bowcock *et al.* (The Muon $g-2$ Collaboration), Phys. Rev. Lett. **131**, 161802 (2023).

[2] L. L. Camilleri, D. C. Cundy, P. Darriulat, J. R. Ellis (CERN), J. Field, H. Fischer, E. Gabathuler,M. K. Gaillard, H. F. Hoffmann, K. Johnsen, E. Keil, F. Palmonari, G. Preparata, B. Richter, C. Rubbia, J. Steinberger, B. H. Wiik, W. J. Willis, and K. Winter, Physics with very high-energy e^+e^- colliding beams, CERN Report No. CERN-76-18, 1976 (CERN, Geneva, 1976), https://doi.org/10.5170/CERN-1976-018.

[3] M. Acciarri, A. Adam, O. Adriani, M. Aguilar-Benitez, S. Ahlen, B. Alpat, J. Alcaraz, J. Allaby, A. Aloisio, G. Alverson, M. G. Alviggi, G. Ambrosi, Q. An, H. Anderhub, V. P. Andreev, T. Angelescu, D. Antreasyan, A. Arefiev, T. Azemoon, T. Aziz *et al.*, Phys. Lett. B **353**, 136 (1995).

[4] M. S. Safronova, D. Budker, D. DeMille, D. F. J. Kimball, A. Derevianko, and C. W. Clark, Rev. Mod. Phys. **90**, 025008 (2018).

[5] P. Zhao, J. R. Lawall, and F. M. Pipkin, Phys. Rev. Lett. **66**, 592 (1991).

[6] E. A. Hessels, P. W. Arcuni, F. J. Deck, and S. R. Lundeen, Phys. Rev. A **46**, 2622 (1992).

[7] T. J. Scholl, R. Cameron, S. D. Rosner, L. Zhang, R. A. Holt, C. J. Sansonetti, and J. D. Gillaspy, Phys. Rev. Lett. **71**, 2188 (1993).

[8] M. Stanke, D. Kędziera, S. Bubin, and L. Adamowicz, Phys. Rev. A **75**, 052510 (2007).

[9] J. Mitroy, S. Bubin, W. Horiuchi, Y. Suzuki, L. Adamowicz, W. Cencek, K. Szalewicz, J. Komasa, D. Blume, and K. Varga, Rev. Mod. Phys. **85**, 693 (2013).

[10] M. Puchalski and K. Pachucki, Phys. Rev. A **73**, 022503 (2006).

[11] I. Hornyák, L. Adamowicz, and S. Bubin, Phys. Rev. A **100**, 032504 (2019).

[12] K. J. Ahrendsen, C. Maruko, K. R. Albert-Aranovich, Q. Berfield-Brewer, A. Esseln, L. Guo, A. E. Ishimwe, Y. Kuzniar, A. E. McKenna, K. J. Soto Villarreal, A. Uprety, L. V. da Silva, K. F. Vogt, and W. D. Williams, Phys. Rev. A **108**, 042815 (2023).

[13] T. Otsuka, T. Suzuki, J. D. Holt, A. Schwenk, and Y. Akaishi, Phys. Rev. Lett. **105**, 032501 (2010).

[14] E. Epelbaum, H.-W. Hammer, and U.-G. Meißner, Rev. Mod. Phys. **81**, 1773 (2009).

[15] J. Carlson, S. Gandolfi, F. Pederiva, S. C. Pieper, R. Schiavilla, K. E. Schmidt, and R. B. Wiringa, Rev. Mod. Phys. **87**, 1067 (2015).

[16] X. Yang, S. Wang, S. Wilkins, and R. G. Ruiz, Prog. Part. Nucl. Phys. **129**, 104005 (2023).

[17] L. Johansson, Ark. Fys. **23**, 119 (1963).

[18] M. Stanke and L. Adamowicz, Phys. Rev. A **100**, 042503 (2019).

[19] M. Puchalski, K. Pachucki, and J. Komasa, Phys. Rev. A **89**, 012506 (2014).

[20] A. Kramida, Y. Ralchenko, J. Reader, and NIST ASD Team, NIST Atomic Spectra Database, version 5.11 (National Institute of Standards and Technology, Gaithersburg, 2023), available at https://physics.nist.gov/asd.

[21] M. Puchalski, J. Komasa, and K. Pachucki, Phys. Rev. A **104**, 022824 (2021).

[22] F. Paschen and P. G. Kruger, Ann. Phys. (Leipzig) **400**, 1005 (1931).

[23] E. C. Cook, A. D. Vira, C. Patterson, E. Livernois, and W. D. Williams, Phys. Rev. Lett. **121**, 053001 (2018).

[24] C. Patterson, A. D. Vira, M. T. Herd, W. B. Hawkins, and W. D. Williams, Rev. Sci. Instrum. **89**, 033107 (2018).

[25] M. Puchalski, J. Komasa, and K. Pachucki, Phys. Rev. A **87**, 030502(R) (2013).

[26] S. Nasiri, L. Adamowicz, and S. Bubin, J. Phys. Chem. Ref. Data **50**, 043107 (2021).

[27] M. T. Herd, C. Maruko, M. M. Herzog, A. Brand, G. Cannon, B. Duah, N. Hollin, T. Karani, A. Wallace, M. Whitmore, and W. D. Williams, J. Opt. Soc. Am. B **39**, 2596 (2022).

[28] V. K. Saini, P. Kumar, K. K. Sarangpani, S. K. Dixit, and S. V. Nakhe, Rev. Sci. Instrum. **88**, 093101 (2017).

[29] I. A. Sulai and P. Mueller, Phys. Rev. A **102**, 042805 (2020).

[30] C. Maruko, N. N. Çölmek, M. T. Herd, K. J. Ahrendsen, B. Cabrales, G. Cannon, E. Davis, X. Y. Guo, T. Karani, A. Wallace, K. Wisnauckas, and W. D. Williams, J. Opt. Soc. Am. B **41**, 1217 (2024).

[31] T. Carette, M. Nemouchi, P. Jönsson, and M. Godefroid, Eur. Phys. J. D **60**, 231 (2010).

[32] P. Jönsson, T. Carette, M. Nemouchi, and M. Godefroid, J. Phys. B **43**, 115006 (2010).

[33] C. J. Sansonetti, C. E. Simien, J. D. Gillaspy, J. N. Tan, S. M. Brewer, R. C. Brown, S. Wu, and J. V. Porto, Phys. Rev. Lett. **107**, 023001 (2011).

[34] R. C. Brown, S. Wu, J. V. Porto, C. J. Sansonetti, C. E. Simien, S. M. Brewer, J. N. Tan, and J. D. Gillaspy, Phys. Rev. A **87**, 032504 (2013).

[35] M. Stanke, J. Komasa, S. Bubin, and L. Adamowicz, Phys. Rev. A **80**, 022514 (2009).

[36] A. Banerjee and V. Natarajan, Opt. Lett. **28**, 1912 (2003).